

# Interference properties of two-component matter wave solitons

Yan-Hong Qin(秦艳红)<sup>1,2</sup>, Yong Wu(伍勇)<sup>3</sup>, Li-Chen Zhao(赵立臣)<sup>1,2,†</sup>, and Zhan-Ying Yang(杨战营)<sup>1,2</sup>

<sup>1</sup>School of Physics, Northwest University, Xi'an 710127, China

<sup>2</sup>Shaanxi Key Laboratory for Theoretical Physics Frontiers, Xi'an 710127, China

<sup>3</sup>School of Public Management, Northwest University, Xi'an 710127, China

(Received 21 October 2019; revised manuscript received 16 December 2019; published online 27 December 2019)

Wave properties of solitons in a two-component Bose–Einstein condensate are investigated in detail. We demonstrate that dark solitons in one of components admit interference and tunneling behavior, in sharp contrast to the scalar dark solitons and vector dark solitons. Analytic analyses of interference properties show that spatial interference patterns are determined by the relative velocity of solitons, while temporal interference patterns depend on the velocities and widths of two solitons, differing from the interference properties of scalar bright solitons. Especially, for an attractive interactions system, we show that interference effects between the two dark solitons can induce some short-time density humps (whose densities are higher than background density). Moreover, the maximum hump value is remarkably sensitive to the variation of the solitons' parameters. For a repulsive interactions system, the temporal-spatial interference periods of dark–bright solitons have lower limits. Numerical simulation results suggest that interference patterns for the dark–bright solitons are more robust against noises than bright–dark solitons. These explicit interference properties can be used to measure the velocities and widths of solitons. It is expected that these interference behaviors can be observed experimentally and can be used to design matter wave soliton interferometer in vector systems.

**Keywords:** solitons, interference behavior, tunneling dynamics, two-component Bose–Einstein condensates

**PACS:** 03.75.Lm, 03.75.Kk, 05.45.Yv, 02.30.Ik

**DOI:** 10.1088/1674-1056/ab65b7

## 1. Introduction

Bose–Einstein condensate (BEC) is a prototypical quantum many-body systems. In the framework of mean-field theory, the dynamics of BEC systems are commonly described by nonlinear Schrödinger equation (NLSE), also known as the Gross–Pitaevskii (GP) equation.<sup>[1]</sup> The atomic interactions are described by a nonlinear term proportional to the  $s$ -wave scattering length and the condensates density. Therefore BECs provide a good platform to study soliton excitations.<sup>[2,3]</sup> Bright solitons,<sup>[4–7]</sup> and dark solitons<sup>[8–11]</sup> are observed in BECs with attractive and repulsive interatomic interactions, respectively. Solitons admit both particle and wave properties. The interactions between solitons are usually elastic just like particles.<sup>[12–14]</sup> Recently, wave properties of solitons were discussed intensively,<sup>[15–24]</sup> mainly including interference behavior and tunneling dynamics, since wave properties can be used to design high-precision matter wave soliton interferometers.<sup>[17–21]</sup> With respect to the interference behavior, some bright soliton interferometers were proposed in BECs with attractive interactions.<sup>[17–21]</sup> The interference and tunneling properties of scalar bright solitons have been described analytically in BECs.<sup>[22,23]</sup> In contrary to the scalar bright solitons, scalar dark solitons do not admit interference or tunneling behavior, due to its effective negative mass nature. However, the dark soliton is another common soliton

excitation, which can be used to measure physical quantities in BECs with repulsive interactions. Therefore, we will discuss the wave properties of vector solitons related to dark soliton in multi-component BECs.

The multi-component coupled systems, far from being a trivial extension of the single-component one, have shown many novel and fundamentally different dynamical behaviors.<sup>[25–31]</sup> Recently, it was shown that tunneling oscillations could be observed between the interaction of two dark solitons in binary repulsive BECs.<sup>[24]</sup> It indicated that dark solitons in one of components can admit wave properties when it is coupled with bright solitons in the other component. Then, it is natural to expect that dark solitons can allow interference behavior in multi-component BECs, and vector solitons can be used to measure more physical parameters than scalar solitons. Therefore, we intend to study interference properties of bright–dark solitons as well as dark–bright solitons in a two-component BECs system. Similar discussions can be extended to more component coupled BECs.

In this paper, we mainly study the interference properties of bright–dark solitons (dark–bright solitons) in a two-component BEC system with attractive (repulsive) interactions. We show that dark solitons in one of components can admit interference and tunneling behavior due to the feedback of the wave properties of bright-soliton component onto the dark one, in sharp contrast to the scalar dark solitons and dark–dark

\*Project supported by the National Natural Science Foundation of China (Grant No. 11775176), the Basic Research Program of the Natural Science of Shaanxi Province, China (Grant No. 2018KJXX-094), the Key Innovative Research Team of Quantum Many-Body Theory and Quantum Control in Shaanxi Province, China (Grant No. 2017KCT-12), and the Major Basic Research Program of the Natural Science of Shaanxi Province, China (Grant No. 2017ZDJC-32).

†Corresponding author. E-mail: zhaolichen3@nwu.edu.cn

solitons. The explicit interference periods are characterized analytically, which suggests that interference patterns can be manipulated precisely by controlling the velocities and widths of the two solitons. For attractive interactions, particularly, we note that the collision of dark solitons can induce some short-time humps above the background density in the dark-soliton component. The detailed analyses show that the maximum hump value of the dark-soliton component is sensitive to the relative phase, relative velocity, and relative width of the two solitons. Additionally, we exhibit tunneling dynamics of solitons in both components. For repulsive interactions, temporal and spatial interference periods are found to have lower limits. The maximum density value of the dark-soliton component is equal to the background, differing substantially from the attractive interactions system. Furthermore, the numerical results show that dark-bright solitons are more robust against noises than bright-dark solitons.

The rest of this paper is arranged as follows. In Section 2, we introduce the theoretical model and present the bright-dark soliton solutions. In Section 3, we analyze in detail the wave properties of two bright-dark solitons during the interaction processes in BECs with attractive interactions, mainly including interference patterns, short-time humps in dark-soliton component, and tunneling dynamics. In Section 4, we explore the interference behavior of dark-bright solitons in BECs with repulsive interactions. The analysis shows that the temporal and spatial interference periods have lower limits. Additionally, we demonstrate the stability of dark-bright solitons by numerical simulations. Finally, we summarize our results in Section 5.

## 2. Theoretical model and bright-dark soliton solutions

In the framework of the mean-field theory, the dynamics of a two-component BEC with attractive interactions can be described well by the following dimensionless coupled NLSE<sup>[32,33]</sup>

$$\begin{aligned} i q_{b,t} + \frac{1}{2} q_{b,xx} + (|q_b|^2 + |q_d|^2) q_b &= 0, \\ i q_{d,t} + \frac{1}{2} q_{d,xx} + (|q_b|^2 + |q_d|^2) q_d &= 0, \end{aligned} \quad (1)$$

where  $q_b(x, t)$  and  $q_d(x, t)$  represent the mean-field wave functions of bright-soliton component and dark-soliton component, respectively. Generally, a dark soliton cannot exist in a system with attractive interactions. But for bright-dark solitons, bright soliton can create an  $-f \operatorname{sech}^2(\sqrt{f}x)$ -type quantum well,<sup>[34,35]</sup> which enables dark soliton to exist as the first-excited state in the quantum well. Therefore, the dark soliton can be described in such an attractive coupled system. The bright-dark solitons have been reported in Refs. [36,37]. To study the collision dynamics of the bright-dark solitons, we re-derive soliton solutions by performing

Darboux transformation<sup>[33,38]</sup> with the seed solutions  $q_{0b} = 0$  and  $q_{0d} = e^{it}$ . For simplicity and without loss of generality, we discuss the collision dynamics of the two bright-dark solitons based on the exact solutions. The two-soliton solutions are

$$\begin{aligned} q_{2b} &= q_{1b} - \frac{i2\lambda_{2i}\Phi_1^*\Phi_2}{|\Phi_1|^2 + |\Phi_2|^2 + |\Phi_3|^2}, \\ q_{2d} &= q_{1d} - \frac{i2\lambda_{2i}\Phi_1^*\Phi_3}{|\Phi_1|^2 + |\Phi_1|^2 + |\Phi_3|^2}, \end{aligned} \quad (2)$$

where  $*$  means the complex conjugation. The explicit expressions for  $\Phi_1$ ,  $\Phi_2$ , and  $\Phi_3$  are presented in Appendix A.  $q_{1b}$  and  $q_{1d}$  are bright-dark one-soliton solutions

$$\begin{aligned} q_{1b} &= w_1 \left[ 1 + \frac{1}{w_1^2 + v_1^2} \right]^{1/2} \operatorname{sech}[w_1(x - v_1t) - \eta/2] e^{i\beta_1 + it}, \\ q_{1d} &= \frac{1}{v_1 - iw_1} \{ v_1 - iw_1 \tanh[w_1(x - v_1t) - \eta/2] \} e^{it}, \\ \eta &= \ln \left( 1 + \frac{1}{v_1 + w_1^2} \right). \end{aligned}$$

Based on the bright-dark two-soliton solutions (2), the asymptotic expressions of  $q_{2b}$  before the collision take the following forms (in the limit  $t \rightarrow -\infty$  with assuming  $v_1 > v_2$ ,  $w_1, w_2 > 0$ ):

$$\begin{aligned} BS_1 &= c_1 \operatorname{sech} \left[ w_1(x - v_1t) + \frac{\eta_1}{2} \right] e^{i\beta_1 + t}, \\ BS_2 &= c_2 \operatorname{sech} \left[ w_2(x - v_2t) + \frac{\eta_2}{2} \right] e^{i\beta_2 + t}, \end{aligned} \quad (3)$$

where  $BS_1$  and  $BS_2$  correspond to the first bright soliton and the second bright soliton in the component  $q_{2b}$  before collisions, respectively,

$$\begin{aligned} \beta_j &= i \left[ v_j x + \frac{1}{2}(w_j^2 - v_j^2)t - \varphi_j \right], \quad j = 1, 2 \\ c_1 &= -iw_1 \frac{(1 + v_1^2 + w_1^2)(v_1 - v_2 + iw_1 - iw_2)}{(v_1^2 + w_1^2)(v_1 - v_2 - iw_1 - iw_2)}, \\ c_2 &= -iw_2 \frac{(1 + v_2^2 + w_2^2)(v_1 - v_2 - iw_1 - iw_2)}{(v_2^2 + w_2^2)(v_1 - v_2 + iw_1 - iw_2)} \\ &\quad \times \frac{(v_1 + iw_1)[1 + (v_1 - iw_1)(v_2 + iw_2)]}{(v_1 - iw_1)[1 + (v_1 + iw_1)(v_2 + iw_2)]}, \\ e^{\eta_1} &= \frac{(v_1^2 + w_1^2)(v_1 - v_2)^2 + (w_1 + w_2)^2}{(1 + v_1^2 + w_1^2)(v_1 - v_2)^2 + (w_1 - w_2)^2}, \\ e^{\eta_2} &= \frac{(v_2^2 + w_2^2)(v_1 - v_2)^2 + (w_1 - w_2)^2}{(1 + v_2^2 + w_2^2)(v_1 - v_2)^2 + (w_1 + w_2)^2} \\ &\quad \times \frac{(v_1 v_2 + 1)^2 + (w_1 w_2 - 1)^2 + v_2^2 w_1^2 + v_1^2 w_2^2 - 1}{(v_1 v_2 + 1)^2 + (w_1 w_2 + 1)^2 + v_2^2 w_1^2 + v_1^2 w_2^2 - 1}. \end{aligned}$$

In the above expressions, the parameters  $v_j$  and  $w_j$  correspond to two soliton velocities and widths respectively.  $\varphi_j$  is the initial phase of the two bright solitons. Based on the asymptotic expressions (3), the peak values of the two bright solitons can be calculated as

$$P_j = w_j \left[ \frac{1 + v_j^2 + w_j^2}{v_j^2 + w_j^2} \right]^{1/2}.$$

It is seen that the peak values of the two bright solitons in the component  $q_{2b}$  are depend on both the widths and velocities of the two solitons. Namely, the amplitude is no longer an independent physical parameter. This is distinct from the case for scalar bright solitons,<sup>[22]</sup> for which the soliton amplitude does not depend on the moving velocity. Therefore, the velocity and width are two independent physical parameters for bright–dark solitons.

### 3. Bright–dark soliton collisions in an attractive interaction system

We study the collision process of two solitons based on the two-soliton solutions Eqs. (2). There are mainly three striking characters: interference patterns, humps induced by dark solitons interactions, and tunneling behavior, in contrast to the scalar dark solitons and dark–dark solitons.<sup>[8–11]</sup> In what follows, we will discuss them separately.

#### 3.1. Interference pattern

As we know, solitons admit both particle and wave properties. The interference behavior is a remarkable characteristics of the wave properties of solitons. The interference properties of scalar bright solitons and bright solitonic matter-wave interferometers have been widely investigated in nonlinear systems.<sup>[17–22,39,40]</sup> However, neither scalar dark solitons nor vector dark solitons admits interference behavior. Interest-

ingly, we note that, during the collision process of bright–dark two solitons, not only the collision between two bright solitons generates the interference pattern in the component  $q_{2b}$ , but two dark solitons’ interplay can also yield the interference pattern in the component  $q_{2d}$ . As an example, we show one case in Fig. 1 by choosing parameters  $v_1 = -2.4$ ,  $v_2 = 1.1$ ,  $w_1 = 0.324$ ,  $w_2 = 0.224$ ,  $\varphi_1 = 0$ , and  $\varphi_2 = 0$ . The top panels show the density distributions of temporal-spatial interference patterns; Figures 1(a) and 1(b) correspond to the component  $q_{2b}$  and the component  $q_{2d}$ , respectively. The bottom panels depict their corresponding spatial interference fringes (at  $t = 0$ , blue solid curve) and temporal interference fringes (at  $x = 1.05$ , red dotted curve). These figures clearly demonstrate the interference behavior of the bright–dark solitons. It is seen that the temporal-spatial interference pattern in the component  $q_{2b}$  gives excellent agreement with scalar scenario in Ref. [22] [see Figs. 1(a), 1(a1) and 1(a2)]. However, the interference behavior is very unusual for dark solitons in the component  $q_{2d}$  [see Figs. 1(b), 1(b1) and 1(b2)], because scalar dark solitons and vector dark solitons do not admit wave properties due to its effective negative mass nature. This indicates that the non-linear interaction between the two components makes the interference behavior in the component  $q_{2b}$  induce the collision of two dark solitons to generate the interference pattern in the component  $q_{2d}$  simultaneously. Namely, due to the feedback of the wave properties of bright soliton onto the dark one, dark solitons can interfere with each other.

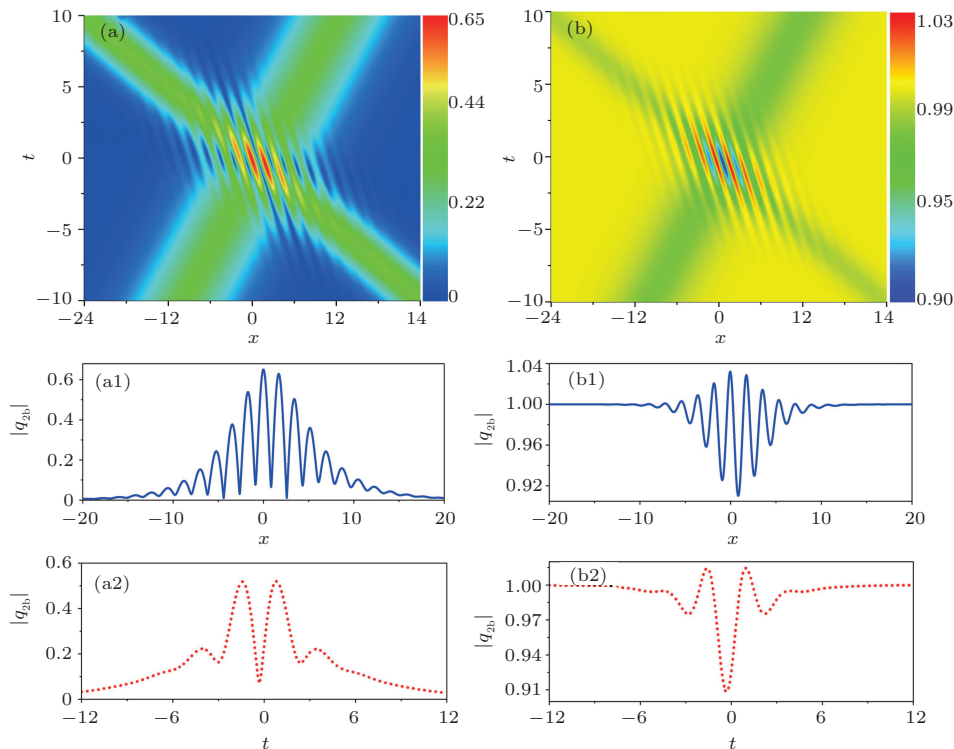


**Fig. 1.** Interference patterns between bright–dark two solitons. Top panel: density evolutions for soliton collisions, panels (a) and (b) correspond to the component  $q_{2b}$  and component  $q_{2d}$ , respectively. Bottom panel: spatial interference fringes (blue solid curve) and temporal interference fringes (red dotted curve); They are the cutaway view of the interference patterns in Figs. 1(a) and 1(b) at  $t = 0$  and  $x = 1.05$ , respectively. Panels (a1) and (a2) correspond to the component  $q_{2b}$ ; panels (b1) and (b2) correspond to the component  $q_{2d}$ . It is shown that the spatial-temporal interference patterns are formed in both components. For dark solitons, interference behavior was absent in the previous studies. The parameters are  $v_1 = -2.4$ ,  $v_2 = 1.1$ ,  $w_1 = 0.324$ ,  $w_2 = 0.224$ ,  $\varphi_1 = 0$ , and  $\varphi_2 = 0$ .

It is important to emphasize that the interference patterns can not always be observed during soliton interaction processes, since the interference periods should be smaller than soliton scales for visible interference fringes.<sup>[22,23]</sup> By means of the asymptotic analysis technique, the spatial and temporal periods are calculated as

$$S = \frac{2\pi}{|v_1 - v_2|}, \quad (4)$$

$$T = \frac{4\pi}{|v_2^2 - v_1^2 + w_1^2 - w_2^2|}, \quad (5)$$

where  $S$  and  $T$  denote spatial period and temporal period, respectively. Obviously, the relative velocity  $(v_1 - v_2)$  determines the spatial interference pattern Eq. (4), while temporal period is determined by both widths  $w_j$  and velocities  $v_j$  of the two solitons Eq. (5). This is quite different from the interference properties of the scalar bright soliton reported previously in Ref. [22], in which temporal period was depended on both the peaks and velocities. By applying the spatial-temporal period expressions Eqs. (4) and (5), the interference patterns can be manipulated by controlling soliton velocities and widths. When the absolute values of velocities of two solitons are identical, the spatial interference pattern will not be formed; When two solitons are of the same width and equal velocity squared, the temporal pattern will disappear. Based on the matter wavelength theory,<sup>[41]</sup> the temporal-spatial interference patterns are visible when the soliton parameters satisfy the condition that spatial period  $S$  is smaller than the scales of two solitons and temporal period  $T$  is smaller than the time scale of collision (as shown in Fig. 1).

Particularly, we note that the two-dark soliton interference effect gives rise to some short-time humps above the background density, as shown in the right panel of Fig. 1, in sharp contrast to scalar dark solitons and dark-dark solitons. This clearly indicates that bright solitons could induce dark solitons to allow much richer dynamics than their own in the repulsive interaction systems. This point is further investigated in the following text.

### 3.2. Maximum hump density value in dark-soliton component

In general, dark solitons collide elastically and could produce some dips in collision region in the repulsive interaction system.<sup>[42]</sup> Nevertheless, we have shown that dark soliton collisions can form some short-time density humps above the background density in the attractive interaction system Eqs. (1), as depicted in the right panel of Fig. 1. To show this character more clearly, we plot Fig. 2 by setting the parameters as  $w_1 = 1.8$ ,  $v_1 = -1$ ,  $w_2 = 1.8$ ,  $v_2 = 1$ ,  $\varphi_1 = 1.8\pi$ , and  $\varphi_2 = 0$ . Figures 2(a1) and 2(b1) correspond to the density evolutions of component  $q_{2b}$  and component  $q_{2d}$ , respectively.

A highlighted feature is that the interactions of the two solitons in both components generate a high hump and two valleys in the collision center simultaneously. Their corresponding intensity profiles at  $t = 0$  (shown in Figs. 2(a2) and 2(b2)) describe clearly this characteristic. Of particular note is that the hump appearing in the component  $q_{2d}$  is significantly higher than the background density. This dynamical behavior is also not admitted for scalar dark solitons and vector dark solitons. It should be mentioned that the humps produced by dark soliton interactions are not always visible. One has to wonder how does the soliton parameters  $w_j, v_j, \varphi_j$  affect the hump values in the component  $q_{2d}$ ? For simplicity, we choose Fig. 2 as an example to discuss the change of maximum hump value of component  $q_{2d}$  at  $t = 0$ , with varying the relative phase, relative velocity, and relative width of the two solitons by means of the control variate method.

Firstly, we study the effect of the relative phase between bright solitons on the maximum density value at  $t = 0$  in the component  $q_{2d}$ . Generally, in a two-soliton circumstance, one soliton can be regarded as the reference ( $\varphi_2 = 0$  herein), and the other soliton initial phase ( $\varphi_1$ ) will become the relative phase (denoted by  $\varphi$ ) between the two bright solitons. Then, one can observe the change of the maximum hump value of component  $q_{2d}$  as the variation of the  $\varphi$  value. As presented in Fig. 3(a),  $\varphi = \varphi_1$  and the other parameters are the same as those given in Fig. 2. Obviously, the hump value  $|q_{2d}|$  is very sensitive to the relative phase  $\varphi$  of the two bright solitons. With the increasing of  $\varphi$ , the hump value of component  $q_{2d}$  appears decreasing at first and then increasing gradually after reaching the minimum hump value (at  $\varphi \approx 0.835\pi$ ) which approximates the background density. Subsequently, the hump value reaches to the maximum value (at  $\varphi \approx 1.835\pi$ ). It indicates that the density distribution of the component  $q_{2d}$  strongly depends on the relative phase between the two bright solitons in the component  $q_{2b}$ . This character could be used to measure the relative phase between solitons.

In the second scenario, we investigate the changes of the maximum hump value of the component  $q_{2d}$  at  $t = 0$  by varying the relative velocity ( $rv$ ) of the two solitons by setting the parameter  $v_1 = v_2 - rv$ , and the other parameters are the same as those in Fig. 2. As shown in Fig. 3(b), there are two critical relative velocities, at  $rv \approx 0.63$  and  $rv \approx 3.91$  respectively. When  $rv \lesssim 0.63$  or  $rv \gtrsim 3.91$ , the change of the maximum density value is nearly imperceptible with the increasing of  $rv$  value. When  $0.63 < rv < 3.91$ , the density value firstly increases to the maximum value at  $rv \approx 1.66$  and then decreases to be very closer to the background density with the increasing of the  $rv$  value. The critical values of relative velocity vary with the relative phase between the bright solitons. The underlying definite properties still need further studies.

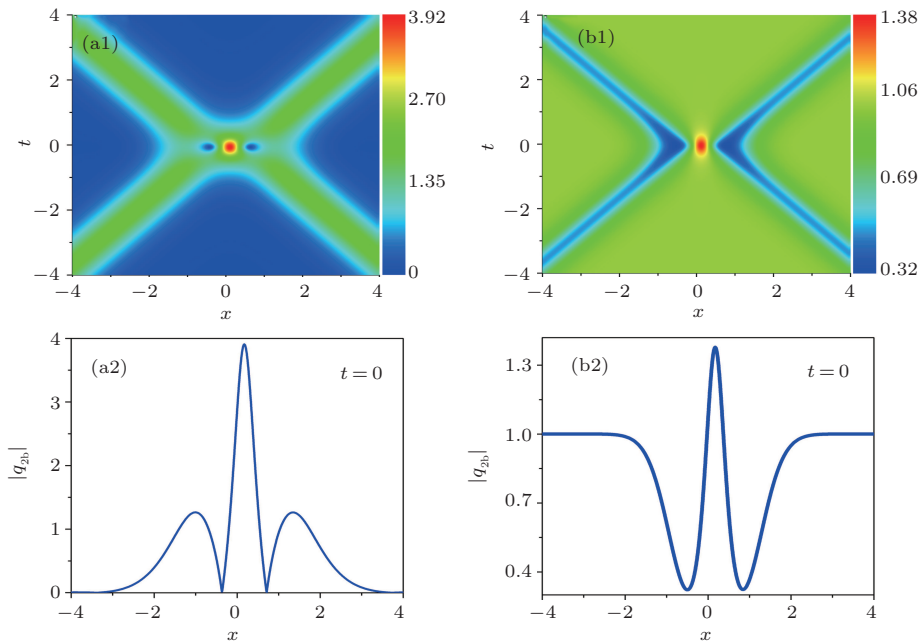


**Fig. 2.** The interaction of bright–dark two solitons. Top panel: density distributions of two solitons collisions in two components; (a1) for component  $q_{2b}$  and (b1) for component  $q_{2d}$ . Bottom panel: intensity profiles for both components at  $t=0$ ; panels (a2) and (b2) correspond to the component  $q_{2b}$  (thin blue curve) and the component  $q_{2d}$  (thick blue curve) respectively. It is seen that the two dark solitons collisions lead to a very high density hump above the background density in component  $q_{2d}$ . The parameters are  $w_1 = 1.8$ ,  $v_1 = -1$ ,  $w_2 = 1.8$ ,  $v_2 = 1$ ,  $\varphi_1 = 1.835\pi$ , and  $\varphi_2 = 0$ .

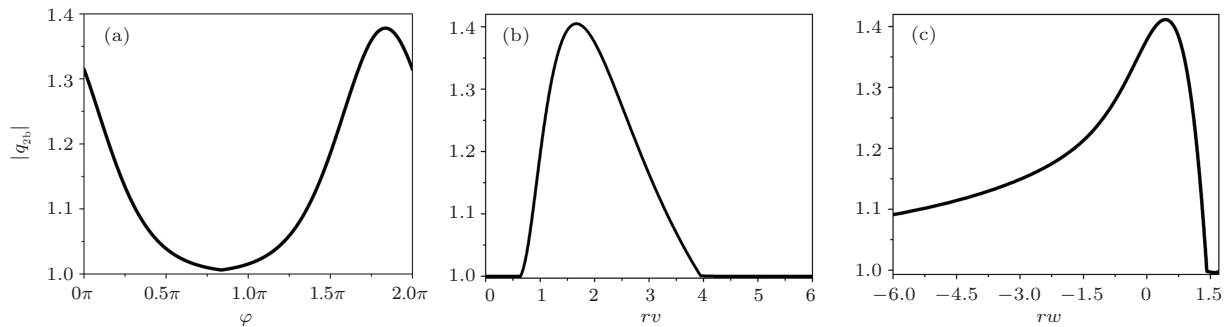


**Fig. 3.** The variation of maximum hump value in dark-soliton component  $q_{2d}$  versus soliton parameters. (a) The maximum hump value varies with the relative phase ( $\varphi$ ) for the choice of parameters  $w_1 = 1.8$ ,  $v_1 = -1$ ,  $w_2 = 1.8$ ,  $v_2 = 1$ ,  $\varphi_1 = \varphi$ , and  $\varphi_2 = 0$ . (b) The maximum hump value varies with the relative velocity ( $rv$ ) between the two solitons, with parameters setting as  $w_1 = 1.8$ ,  $v_1 = v_2 - rv$ ,  $w_2 = 1.8$ ,  $v_2 = 1$ ,  $\varphi_1 = 1.835\pi$ , and  $\varphi_2 = 0$ . (c) The maximum hump value varies with the relative width ( $rw$ ) between the two solitons with parameters  $w_1 = w_2 - rw$ ,  $v_1 = -1$ ,  $w_2 = 1.8$ ,  $v_2 = 1$ ,  $\varphi_1 = 1.835\pi$ , and  $\varphi_2 = 0$ . It is shown that the maximum density hump value is very sensitive to soliton parameters.

Thirdly, we investigate the change of the maximum hump value of component  $q_{2d}$  at  $t=0$  by varying the relative width ( $rw$ ) between the two solitons by setting parameters  $w_1 = w_2 - rw$  and the other parameters are the same as those in Fig. 2. This is depicted in Fig. 3(c). Note that the maximum density value becomes progressively discernible as the increasing of  $rw$  value. When the difference between their width value keeps decreasing, the maximum density value continues to increase. When  $rw \approx 0.44$ , the density of the component  $q_{2b}$  reaches the highest value. With further increasing the  $rw$  value, the width of the first soliton tends to be very small, the maximum density value decreases rapidly being close to the background density. This reveals that the scales of the two solitons dramatically affect the density distribution of the component  $q_{2d}$ . It should be pointed out that when the relatively velocity of the two solitons is relatively large, the change of the  $rw$  value has no significant effect on

the maximum density value of the component  $q_{2d}$ .

More recently, a method was proposed to split the ground state of an attractively interacting BEC into two bright solitary waves with controlled relative phase and velocity.<sup>[43]</sup> Combining the above discussions, one expects these properties could be used to test some physical quantities related to solitons in the near-future experiments.

### 3.3. Tunneling behavior

The quantum tunneling dynamics of solitons have been discussed well in Refs. [23,24,44–49]. Recently, tunneling dynamics of dark solitons in a harmonic trap were investigated in binary repulsive BECs,<sup>[24]</sup> based on different initial conditions of the phase difference and population imbalance of the bright solitons. Then, it would be natural to expect that the tunneling dynamics between dark solitons can also be observed in the coupled system Eqs. (1).

Based on the quantum tunneling theory,<sup>[50]</sup> the nonlinear term  $-(|q_b|^2 + |q_d|^2)$  in Eqs. (1) can be seen as an effective double-well potential, which is self-induced by the distribution of atoms. The structure of quantum wells evolve simultaneously with the evolution of bright solitons and dark solitons in both components, since atoms tunneling from one soliton to the other change the quantum well structure synchronously. Therefore, we call it as the tunneling behavior of matter-wave solitons in a self-induced quantum wells, in contrast to the external double-well potential in usual quantum theory. One of the typical examples of the density for tunneling behavior is depicted in Fig. 4 by setting the parameters  $w_1 = 2.9$ ,  $v_1 = -0.05$ ,  $w_2 = 3.9$ ,  $v_2 = 0.05$ ,  $\phi_1 = \phi_2 = 0$ , panels (a) and (b) correspond to component  $q_{2b}$  and component  $q_{2d}$  respectively. It is seen that the coupled nonlinear effects between the two components force dark solitons performing periodic oscillation in time evolution together with the bright solitons. In contrary, scalar dark solitons and dark-dark solitons do not allow these features due to its effective negative mass nature. The tunneling period is calculated as  $T = 4\pi/|v_2^2 - v_1^2 + w_1^2 - w_2^2|$ , determined by widths and velocities of solitons. For visible tunneling behavior, the tunneling period should be smaller than the half of time scale of collision. Tunneling dynamics shown in Fig. 4 is different from those observed in Ref. [24], in which oscillations were related with the deviation from the in-phase or out-of-phase stationary solution.

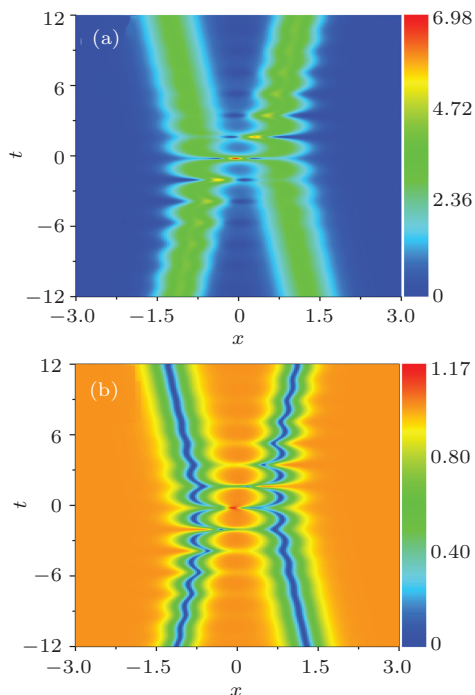


**Fig. 4.** The tunneling behavior between the two bright-dark solitons. Panel (a) shows the density of the bright-soliton component, (b) for the dark-soliton component. It is seen that the oscillating tunneling behavior emerges during the interaction process. Parameters are  $w_1 = 2.9$ ,  $v_1 = -0.05$ ,  $w_2 = 3.9$ ,  $v_2 = 0.05$ , and  $\phi_1 = \phi_2 = 0$ .

Next, we simulate the evolutions of the bright-dark solitons in the coupled system (1) to test their stability by the dis-

crete cosine transform method with homogeneous Neumann boundary conditions.<sup>[51]</sup> The numerical evolution results of the bright-dark solitons are displayed in Fig. 5, which initial excitation forms are given by the same parameters of Fig. 1 at  $t = -7$ , panel (a) for component  $q_{2b}$  and (b) for component  $q_{2d}$ . It is seen that the numerical results in Fig. 5 reproduce the interference fringes with high visibility when solitons collide with each other in both components, which agrees pretty well with the analytical results in Figs. 1(a) and 1(b). However, there are some other localized waves emerging in dark-soliton component when  $t \gtrsim 1.5$ , induced by the modulational instability of the background fields.<sup>[52]</sup> In view of this fact, we would like to further investigate the interference behavior of the dark-bright solitons in two-component BECs with repulsive interactions, since the background field does not admit any modulational instability.

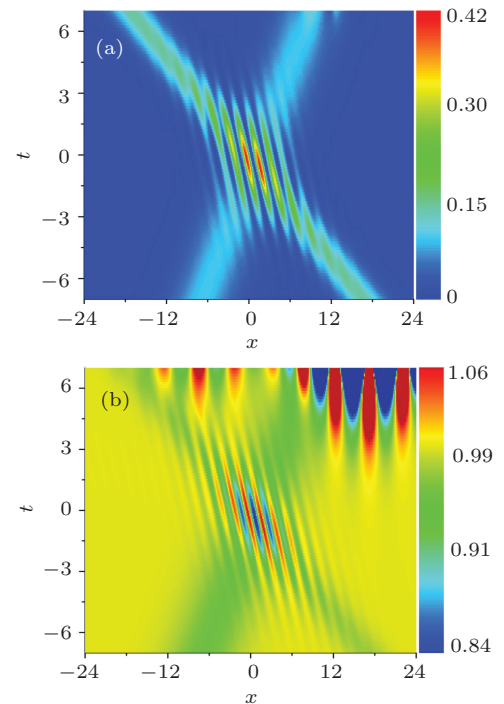


**Fig. 5.** Numerical simulations of the bright-dark solitons with the same parameters as given in Fig. 1: (a) for bright-soliton component  $q_{2b}$ , and (b) for dark-soliton component  $q_{2d}$ . It is seen that the background density presents to be unstable in the dark-soliton component  $q_{2d}$  after the time  $t \approx 1.5$ .

#### 4. Dark-bright soliton interference in repulsive interaction system

For the dark-bright solitons in a two-component BECs with repulsive interactions, the dark solitons in one of components play the role of an effective potential that enables the bound-state trapping of the bright-soliton component.<sup>[10,53–55]</sup> It is expected that the dark solitons can show more exotic dynamics behaviors in this system, coupled with bright solitons. We consider the two-component coupled NLSE with repulsive

interactions of the forms

$$\begin{aligned} i q_{d,t} + q_{d,xx} - 2(|q_d|^2 + |q_b|^2)q_d &= 0, \\ i q_{b,t} + q_{b,xx} - 2(|q_d|^2 + |q_b|^2)q_b &= 0. \end{aligned} \quad (6)$$

The dynamics of the two dark–bright solitons can be described by the well-known exact solutions in Ref. [54]

$$\begin{aligned} q_d = q_0 e^{-2i q_0^2 t} \left\{ 1 + \frac{1}{D} \left[ \frac{\Gamma_1}{z_1(z_1^* - z_1)} + \frac{\Gamma_2}{z_2(z_2^* - z_2)} \right. \right. \\ \left. \left. + \Gamma_3 \frac{e^{-i\beta}(q_0^2 - z_1^* z_2) \delta_1^* \delta_2}{z_2(z_2 - z_1^*)} + \Gamma_3 \frac{e^{i\beta}(q_0^2 - z_1 z_2^*) \delta_1 \delta_2^*}{z_1(z_1 - z_2^*)} \right. \right. \\ \left. \left. + \frac{z_1^* z_2^* - z_1 z_2}{z_1 z_2} \Gamma_5 \right] \right\}, \end{aligned} \quad (7)$$

$$\begin{aligned} q_b = -\frac{q_0 e^{-2i q_0^2 t}}{D} \left[ \frac{\bar{\delta}_1 z_1^*}{q_0^2} e^{-i z_1^*(x+z_1^* t)} + \frac{\bar{\delta}_2 z_2^*}{q_0^2} e^{-i z_2^*(x+z_2^* t)} \right. \\ \left. + \Gamma_4 \frac{\bar{\delta}_1 \bar{\delta}_2 z_1^* z_2^* (q_0^2 - z_1^* z_2^*) (z_1^* - z_2^*)^2}{q_0^2 (q_0^2 - z_1 z_2)} \right], \end{aligned} \quad (8)$$

where the explicit expressions for  $D$ ,  $\bar{\delta}_{1,2}$ , and  $\Gamma_i$  ( $i = 1, 2, \dots, 5$ ) are presented in Appendix A.  $q_d(x, t)$  and  $q_b(x, t)$  describe the wave functions of the dark-soliton component and the bright-soliton component, respectively.  $q_0$  is the amplitude of background.  $z_j = \kappa_j + i\rho_j$  corresponds to the eigenvalues of the inverse scattering transform problem with  $|z_j| < q_0$ ,  $j = 1, 2$ . The soliton velocity is  $v_j = 2\kappa_j$ .  $\delta_j = 2\rho_j/[q_0(q_0^2 - z_j^2)^{1/2}] e^{x_j + i\phi_j}$  is the so-called norming constants. The position offset and phase of solitons are described by  $x_j$  and  $\phi_j$  respectively.

The dark–bright solitons in the repulsive interactions system Eqs. (6) have similar wave properties to the bright–dark solitons in the attractive interactions system Eqs. (1), such as interference behavior and tunneling dynamics. As an example, herein we show their interference patterns with high visibility in both components shown in Fig. 6: panel (a) for component  $q_d$  and (b) for component  $q_b$  (see the caption for details). By further simplifying soliton solutions (7) and (8) and combining the asymptotic analysis expressions in Ref. [54], the interference periods can be obtained. The spatial interference period is  $S = 4\pi/|v_1 - v_2|$ , and temporal interference period is

$$T = 2\pi/|w_1^2 - w_2^2 - (1/4)(v_1^2 - v_2^2)|,$$

where  $w_1$  and  $w_2$  are the widths of the two solitons with  $w_j = \rho_j$ . It is shown that the spatial interference period depends on the relative velocity of the two solitons, and the temporal interference period is determined by the velocities and widths of the two solitons (herein the parameter settings in Fig. 6 make the temporal period be zero). Their interference properties are similar to the bright–dark solitons mentioned in

Section 3. But it must be emphasized that interference periods of the dark–bright solitons are found to have lower limits, namely,  $S > \pi/q_0$  and  $T > \pi/q_0^2$ . This is induced by the velocity of the dark soliton, it is always lower than the sound speed of the system for the dark–bright soliton, and is different from the bright–dark soliton as mentioned above. Moreover, we note that the maximum density value of the dark-soliton component is always equal to the background density, in stark contrast to bright–dark solitons in attractive interaction system (comparing Fig. 1(b) and Fig. 2(b1) to Fig. 6(a)).

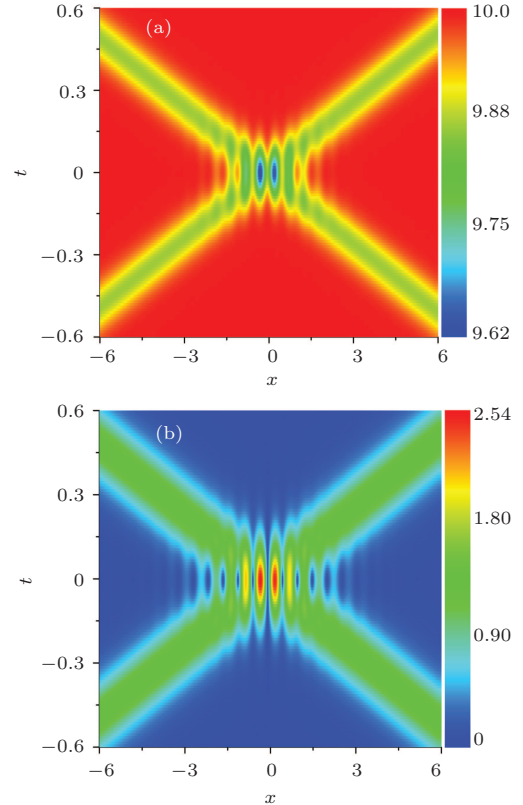


**Fig. 6.** Interference patterns of the two dark–bright soliton interactions: (a) for dark-soliton component and (b) for bright-soliton component. The parameters are  $\rho_1 = \rho_2 = 1$ ,  $\kappa_1 = -\kappa_2 = -6$ ,  $q_0 = 10$ ,  $x_1 = x_2 = 0$ , and  $\phi_1 = \phi_2 = \pi/4$ .

We further perform numerical simulations to verify the stability of the dark–bright solitons.<sup>[51]</sup> In the present study, we simulate the initial excitation condition perturbed with 2% white noise of small amplitudes. Namely, we multiply the  $q_d$  and  $q_b$  by the factor  $(1 + 0.02 \text{Random}[-1, 1])$ . For instance, we show the simulation results for the two dark–bright solitons as shown in Fig. 7. The initial excitation forms are given by the exact ones at  $t = -0.5$  in Fig. 6 with adding small noise. It is seen that, under the noise perturbation, simulation results reproduce the stable interference patterns in both components, which agree well with the analytical results shown in Fig. 6. It reveals that the dark–bright solitons are very robust against perturbations than the bright–dark solitons since there is no modulational instability for the repulsive interaction system Eqs. (6).

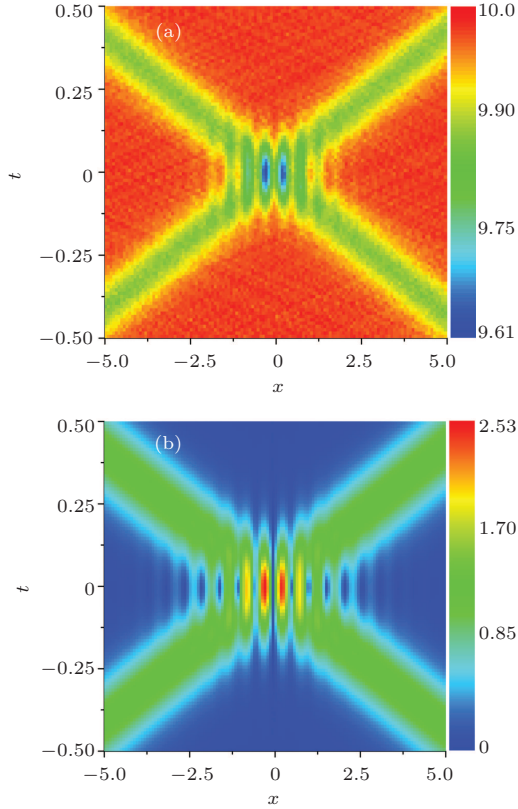


**Fig. 7.** The numerical simulations of the dark–bright solitons with small noise: (a) for dark-soliton component and (b) for bright-soliton component. The initial excitation conditions are given by the same parameters as in Fig. 6 at  $t = -0.5$  by multiplying a factor  $(1 + 0.02 \text{Random}[-1, 1])$ . It is seen that the dark–bright solitons are robust against small noise.

## 5. Conclusion and Discussion

In this paper, we show that interactions between the bright–dark two-soliton (attractive interactions) and the dark–bright two-soliton (repulsive interactions) both can generate temporal-spatial interference patterns, which are not admitted for scalar dark solitons and vector dark solitons. The explicit interference periods expressions can be used to measure some physical quantities, such as soliton velocity, width, and related acceleration fields. In the attractive interaction system, the maximum density value of the dark-soliton component can be higher than the background density and changes obviously as the variation of soliton parameters. Additionally, we display the tunneling dynamics of the bright–dark solitons. In the

repulsive interactions system, since soliton’s velocity cannot exceed the speed of sound, the spatial-temporal interference periods both have lower limits. Moreover, we use numerical simulations to test the stabilities of the bright–dark solitons and dark–bright solitons. The results indicate that the dark–bright solitons are more robust than the bright–dark solitons as the background field does not admit any modulational instability for the repulsive system. From a physical perspective, the nonlinear feedback of the bright soliton into the dark soliton leads the latter to admit more interesting dynamics in the other component, rather than only retaining the characters as scalar dark solitons or dark–dark solitons.

Experimentally, dark solitons are prepared firstly and then provide an effective potential to excite bright solitons, for dark–bright solitons in BEC with repulsive interactions.<sup>[10,55]</sup> Based on the well-developed density and phase modulation techniques in BECs,<sup>[4–11]</sup> the bright–dark solitons could be observed in BEC with attractive interactions. To excite bright–dark solitons, one should prepare bright soliton firstly and then dark soliton can be excited as the first-excited state in the effective quantum well created by the bright-soliton component.<sup>[34]</sup> As far as we know, the bright–dark solitons have not been observed in BEC systems, mainly due to the modulational instability of the dark soliton background. Moreover, soliton interactions have been also demonstrated experimentally in BECs.<sup>[16,43]</sup> Recently, interferometer with BECs in microgravity,<sup>[56]</sup> spin–orbit coupled interferometer,<sup>[57]</sup> and multicomponent interferometer in a spinor BECs<sup>[58]</sup> were proposed, which demonstrate that the interference pattern holds great promise for implementing quantum tests and measurement information for uncorrelated systems. One can expect that the interference patterns and tunneling behavior of vector solitons obtained here can be used to measure some physical quantities in some ultra-cold atomic gases.

## Appendix A

The explicit expressions for  $\Phi_1$ ,  $\Phi_2$ ,  $\Phi_3$  of Eqs. (2) are as follows:

$$\begin{aligned}\Phi_1 &= \frac{\lambda_2 \Phi_{21}}{\lambda_2 - \lambda_1^*} + \frac{\lambda_1 \Phi_{11}(\Phi_{11}^* \Phi_{21} + \Phi_{12}^* \Phi_{22} + \Phi_{13}^* \Phi_{23}) + \lambda_1^*[(|\Phi_{12}|^2 + |\Phi_{13}|^2)\Phi_{21} - (\Phi_{12}^* \Phi_{22} + \Phi_{13}^* \Phi_{23})\Phi_{11}^*]}{(\lambda_1^* - \lambda_2)(|\Phi_{11}|^2 + |\Phi_{12}|^2 + |\Phi_{13}|^2)}, \\ \Phi_2 &= \frac{\lambda_2 \Phi_{22}}{\lambda_2 - \lambda_1^*} + \frac{\lambda_1 \Phi_{12}(\Phi_{11}^* \Phi_{21} + \Phi_{12}^* \Phi_{22} + \Phi_{13}^* \Phi_{23}) + \lambda_1^*[(|\Phi_{11}|^2 + |\Phi_{13}|^2)\Phi_{22} - (\Phi_{11}^* \Phi_{11} + \Phi_{13}^* \Phi_{23})\Phi_{12}^*]}{(\lambda_1^* - \lambda_2)(|\Phi_{11}|^2 + |\Phi_{12}|^2 + |\Phi_{13}|^2)}, \\ \Phi_3 &= \frac{\lambda_2 \Phi_{23}}{\lambda_2 - \lambda_1^*} + \frac{\lambda_1 \Phi_{13}(\Phi_{11}^* \Phi_{21} + \Phi_{12}^* \Phi_{22} + \Phi_{13}^* \Phi_{23}) + \lambda_1^*[(|\Phi_{11}|^2 + |\Phi_{12}|^2)\Phi_{23} - (\Phi_{11}^* \Phi_{21} + \Phi_{12}^* \Phi_{22})\Phi_{13}^*]}{(\lambda_1^* - \lambda_2)(|\Phi_{11}|^2 + |\Phi_{12}|^2 + |\Phi_{13}|^2)},\end{aligned}$$

where  $\Phi_{j1} = e^{\alpha_j - i\beta_j}$ ,  $\Phi_{j2} = e^{it}$ ,  $\Phi_{j3} = (e^{\alpha_j - i\beta_j + it})/(i w_j - v_j)$ ,  $\alpha_j = w_j(x - v_j t)$ ,  $\beta_j = v_j x - (1/2)(v_j^2 - w_j^2)t - \varphi_j$ ,  $\lambda_j = \lambda_{jr} + i\lambda_{ji}$ ,  $\lambda_{ji} = w_j [1/(v_j^2 + w_j^2) + 1]$ ,  $\lambda_{jr} = v_j [1/(v_j^2 + w_j^2) - 1]$ ,  $j = 1, 2$ .

The expressions for  $\bar{\delta}_{1,2}$ ,  $D$ , and  $\Gamma_i$  of Eqs. (7) and (8) are

$$\begin{aligned} \bar{\delta}_1 &= -\frac{q_0^2(q_0^2 - |z_1|^2)(q_0^2 - z_1^*z_2)}{(z_1^*)^2(q_0^2 - z_1^*z_2^*)} \delta_1^*, & \bar{\delta}_2 &= -\frac{q_0^2(q_0^2 - |z_2|^2)(q_0^2 - z_1z_2^*)}{(z_2^*)^2(q_0^2 - z_1^*z_2^*)} \delta_2^*, \\ \Gamma_1 &= \frac{q_0^2(q_0^2 - |z_1|^2)|q_0^2 - z_1^*z_2|^2|\delta_1|^2}{|q_0^2 - z_1z_2|^2} e^{-2\rho_1\xi_1}, & \Gamma_2 &= \frac{q_0^2(q_0^2 - |z_2|^2)|q_0^2 - z_1^*z_2|^2|\delta_2|^2}{|q_0^2 - z_1z_2|^2} e^{-2\rho_2\xi_2}, \\ \Gamma_3 &= \frac{q_0^2(q_0^2 - |z_1|^2)(q_0^2 - |z_2|^2)}{|q_0^2 - z_1z_2|^2} e^{-(\rho_1\xi_1 + \rho_2\xi_2)}, & \Gamma_4 &= \frac{\delta_1z_1 e^{-2\rho_1\xi_1 - iz_2^*(x+z_2^*t)}}{(z_1^* - z_1)^2(z_1 + z_2^*)^2} + \frac{\delta_2z_2 e^{-2\rho_2\xi_2 - iz_1^*(x+z_1^*t)}}{(z_2^* - z_2)^2(z_2 - z_1^*)^2}, \\ \Gamma_5 &= \frac{(q_0^2 - |z_1|^2)(q_0^2 - |z_2|^2)|q_0^2 - z_1^*z_2|^2|z_1 - z_2|^4}{16\rho_1^2\rho_2^2|q_0^2 - z_1z_2|^2|z_1^* - z_2|^4} \times q_0^4|\delta_1|^2|\delta_2|^2 e^{-2(\rho_1\xi_1 + \rho_2\xi_2)}, \quad (\xi_j = x + 2\kappa_j t, j = 1, 2), \\ D &= \Gamma_3 \left[ \frac{-e^{i\beta}(q_0^2 - z_1z_2^*)\delta_1\delta_2^*}{(z_1 - z_2^*)^2} - \frac{e^{-i\beta}(q_0^2 - z_1^*z_2)\delta_1^*\delta_2}{(z_2 - z_1^*)^2} \right] + 1 + \frac{\Gamma_1}{4\rho_1^2} + \frac{\Gamma_2}{4\rho_2^2} + \Gamma_4. \end{aligned}$$

## References

- [1] Gross E P 1961 *Nuovo Cimento* 20 454 Pitaevskii L P 1961 *Sov. Phys. JETP* 13 451
- [2] Pitaevskii L P and Stringari S 2003 *Bose-Einstein Condensation* (Oxford: Oxford University Press)
- [3] Kevrekidis P G, Frantzeskakis D J and Carretero-González R 2007 *Emergent Nonlinear Phenomena in Bose-Einstein Condensates: Theory and Experiment* (Berlin, Heidelberg: Springer)
- [4] Strecker K E, Partridge G B, Truscott A G and Hulet R G 2002 *Nature* 417 150
- [5] Khaykovich L, Schreck F, Ferrari G, Bourdel T, Cubizolles J, Carr L D, Castin Y and Salomon C 2002 *Science* 296 1290
- [6] Cornish S L, Thompson S T and Wieman C E 2006 *Phys. Rev. Lett.* 96 170401
- [7] Marchant A L, Billam T P, Wiles T P, Yu M M H, Gardiner S A and Cornish S L 2013 *Nat. Commun.* 4 1865
- [8] Burger S, Bongs K, Dettmer S, Ertmer W, Sengstock K, Sanpera A, Shlyapnikov G V and Lewenstein M 1999 *Phys. Rev. Lett.* 83 5198
- [9] Denschlag J, Simsarian J E, Feder D L, et al. 2000 *Science* 287 97
- [10] Becker C, Stellmer S, Soltan-Panahi P, Dörscher S, Baumert M, Richter E M, Kronjäger J, Bongs K and Sengstock K 2008 *Nat. Phys.* 4 496
- [11] Weller A, Ronzheimer J P, Gross C, Esteve J, Oberthaler M K, Frantzeskakis D J, Theocharis G and Kevrekidis P G 2008 *Phys. Rev. Lett.* 101 130401
- [12] Salle M A and Matveev V B 1991 *Darboux transformations and solitons* (Berlin: Springer-Verlag)
- [13] Akhmediev N and Ankiewicz A 1993 *Opt. Commun.* 100 186
- [14] Zhang X F, Hu X H, Liu X X and Liu W M 2009 *Phys. Rev. A* 79 033630
- [15] Zhao L C, Xin G G and Yang Z Y 2017 *J. Opt. Soc. Am. B* 34 2569
- [16] Nguyen J H V, Dyke P, Luo D, Malomed B A and Hulet R G 2014 *Nat. Phys.* 10 918
- [17] McDonald G D, Kuhn C C N, Hardman K S, et al. 2014 *Phys. Rev. Lett.* 113 013002
- [18] Polo J and Ahufinger V 2013 *Phys. Rev. A* 88 053628
- [19] Negretti A and Henkel C 2004 *J. Phys. B: At. Mol. Opt. Phys.* 37 385
- [20] Helm J L, Cornish S L and Gardiner S A 2015 *Phys. Rev. Lett.* 114 134101
- [21] Zhao L C, Xin G G, Yang Z Y and Yang W L "Atomic bright soliton interferometry", arXiv: 1804.01951
- [22] Zhao L C, Ling L, Yang Z Y and Liu J 2016 *Nonlinear Dyn.* 83 659
- [23] Zhao L C, Ling L, Yang Z Y and Yang W L 2017 *Nonlinear Dyn.* 88 2957
- [24] Karamatskos E T, Stockhofe J, Kevrekidis P G and Schmelcher P 2015 *Phys. Rev. A* 91 043637
- [25] Busch Th, Cirac J I, Pérez-García V M and Zoller P 1997 *Phys. Rev. A* 56 2978
- [26] Liu X, Pu H, Xiong B, Liu W M and Gong J 2009 *Phys. Rev. A* 79 013423
- [27] Wang L X, Dai C Q, Wen L, Liu T, Jiang H F, Saito H, Zhang S G and Zhang X F 2018 *Phys. Rev. A* 97 063607
- [28] Xu T and Chen Y 2018 *Commun. Nonlinear Sci. Numer. Simulat.* 57 276
- [29] Wang M and Chen Y 2019 *Nonlinear Dyn.* 98 1781
- [30] Qin Y H, Zhao L C and Ling L M 2019 *Phys. Rev. E* 100 022212
- [31] Charalampidis E G, Wang W, Kevrekidis P G, Frantzeskakis D J and Cuevas-Maraver J 2016 *Phys. Rev. A* 93 063623
- [32] Guo B L and Ling L M 2011 *Chin. Phys. Lett.* 28 110202
- [33] Ling L and Zhao L C 2019 *Commun. Nonlinear Sci. Numer. Simulat.* 72 449
- [34] Zhao L C, Yang Z Y and Yang W L 2019 *Chin. Phys. B* 28 010501
- [35] Akhmediev N and Ankiewicz A 1999 *Phys. Rev. Lett.* 82 2661
- [36] Vijayajayanthi M, Kanna T and Lakshmanan M 2008 *Phys. Rev. A* 77 013820
- [37] Ling L, Zhao L C and Guo B 2016 *Commun. Nonlinear Sci. Numer. Simulat.* 32 285
- [38] Guo B, Ling L and Liu Q P 2012 *Phys. Rev. E* 85 026607
- [39] Snyder A W and Mitchell D J 1997 *Science* 276 1538
- [40] Kumar V R, Radha R and Panigrahi P K 2009 *Phys. Lett. A* 37 4381
- [41] Belyaeva T L and Serkin V N 2012 *Eur. Phys. J. D* 66 153
- [42] Ling L, Zhao L C and Guo B L 2015 *Nonlinearity* 28 3243
- [43] Billam T P, Cornish S L, and Gardiner S A 2011 *Phys. Rev. A* 83 041602
- [44] Barak A, Peleg O, Stucchio C, Soffer A and Segev M 2008 *Phys. Rev. Lett.* 100 153901
- [45] Serkin V N, Chapelaa V M, Percinoia J and Belyaevab T L 2001 *Opt. Commun.* 192 237
- [46] Serkin V N, Hasegawa A and Belyaeva T L 2013 *J. Mod. Opt.* 60 116
- [47] Serkin V N, Hasegawa A and Belyaeva T L 2013 *J. Mod. Opt.* 60 444
- [48] Martin A D and Ruostekoski J 2012 *New. J. Phys.* 14 043040
- [49] Tkeshelashvili L 2012 *Phys. Rev. A* 86 033836
- [50] Josephson B D 1962 *Phys. Lett.* 1 251
- [51] Bao W, Tang Q and Xu Z 2013 *J. Comput. Phys.* 235 423
- [52] Tai K, Hasegawa A and Tomita A 1986 *Phys. Rev. Lett.* 56 135
- [53] Busch Th and Anglin J R 2001 *Phys. Rev. Lett.* 87 010401
- [54] Dean G, Klotz T, Prinari B and Vitale F 2013 *Appl. Anal.* 92 379
- [55] Hamner C, Chang J J, Engels P and Hoefler M A 2011 *Phys. Rev. Lett.* 106 065302
- [56] Müntinga H, Ahlers H, Krutzik M, et al. 2013 *Phys. Rev. Lett.* 110 093602
- [57] Helm J L, Billam T P, Rakonjac A, Cornish S L and Gardiner S A 2018 *Phys. Rev. Lett.* 12 063201
- [58] Tang P, Peng P, Li Z, Chen X, Li X and Zhou X 2019 *Phys. Rev. A* 100 013618